공학석사학위논문

Silver Nanowire Electrodes in Organic Solar Cells

유기태양전지용 은 나노선 전극

2014 년 **5** 월

서울대학교 대학원

전기 정보 공학부

Felix Penningsfeld

공학석사학위논문

Silver Nanowire Electrodes in Organic Solar Cells

유기태양전지용 은 나노선 전극

2014 년 **5** 월

서울대학교 대학원

전기 정보 공학부

Felix Penningsfeld

Silver Nanowire Electrodes in Organic Solar Cells

지도교수 이창희

이 논문을 공학석사 학위논문으로 제출함

2014 년 5 월

서울대학교 대학원

전기 정보 공학부

Felix Penningsfeld

Felix Penningsfeld 의 공학석사 학위논문을 인준함

2014 년 5 월

위 원 장 : _____(인)

부위원장 : _____(인)

위　　원 : _____(인)

ABSTRACT

Silver Nanowire Electrodes in Organic Solar Cells

Felix Penningsfeld
Department of Electrical and Computer Engineering
College of Engineering
Seoul National University

Transparent electrodes are an essential part of photoactive and light emitting devices. The currently widespread use of Indium Tin Oxide (ITO) as transparent conductive electrode in organic solar cells is not suited for commercial application. High material costs, high processing temperatures, and low mechanical durability of ITO are an obstacle for the advancement of organic solar cell technology.

Therefore, alternatives for ITO, such as conducting polymers, metal nanowires, and carbon nanotubes have increasingly been researched in organic electronics. Among these silver nanowire films show superior mechanical stability, high optical transmittance, as well as good conductivity. Combined with low material and

manufacturing costs, silver nanowire networks are the most promising alternative to ITO.

In this thesis we are illustrating the implementation of silver nanowires from the principles of nanowire synthesis to the final application in organic solar cells in a laboratory environment.

We investigate the physical principles of percolative networks as well as processing methods involved in producing high performing electrodes. Exploration of material properties and performance measurement under real-life conditions show challenges and hurdles that still have to be overcome. We introduce an alternative patterning method for electrodes and conduct experiments with additives to enhance performance of silver nanowire electrodes.

As a result, we demonstrate organic solar cells based on silver nanowires as a low-cost, flexible alternative to ITO with equivalent performance, and deliver guidance to a better understanding of the working mechanics behind nanowire networks that will help to advance organic photovoltaic devices.

Keywords : organic solar cell, silver nanowire, electrode

Student Number : 2012-23965

TABLE OF CONTENTS

LIST OF FIGURES

LIST OF TABLES

1 INTRODUCTION

With the advances in science and technology the worldwide demand for electricity and power in general has increased tremendously over the last decades[1]. Among the many reasons for the increased demand, some can be found in the industrialization of manufacturing and the progressing digitalization of society with computers and other electronic devices. Among the *OECD* (Organization for Economic Co-operation and Development) countries, South Korea showed an extraordinary development in economic growth and technological advancement since the 1960s, which is often described as the 'Miracle on the Han'[2]. This development went hand in hand with an increasing demand in energy to fuel the continuing economic growth. The *iea* (International Energy Agency) reports the South Korean total primary energy consumption as nearly 12 quadrillion *btu* (British Thermal Unit) in the year 2012[3], ranking South Korea among the top 10

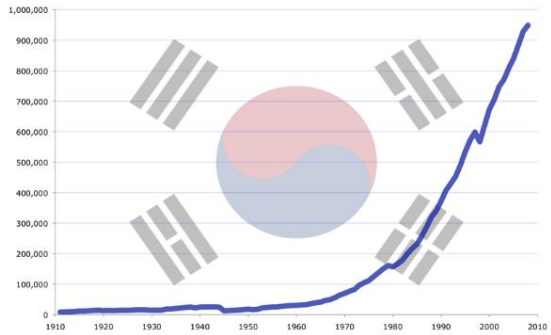

Figure 1 South Korea's GDP growth from 1911 to 2008 [61]

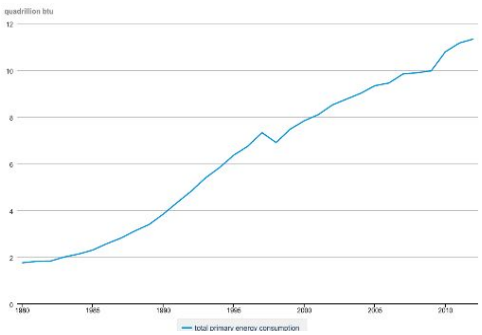

Figure 2 Rise of total energy consumption in South Korea from 1980-2012 [1]

consumer countries worldwide.

To cover the increasing energy demand, mainly fossil fuels like coal, petroleum, and natural gases are used (Figure 3). Fossil fuels are not only limited in supply but the conversion process to energy also leads to a tremendous build-up of CO_2 in the

atmosphere and contamination of air with fine dust particles, which poses an increasing threat to public health[4].

To minimize negative effects of fossil fuel conversion, alternative ways to provide energy to consumers and industries are being researched and deployed. Sustainable energy sources, also known as 'Green energy', are technologies based on renewable energy sources, such as wind energy, solar energy, hydroelectricity, tidal power and others[5]. To enhance energy security and diversify energy sources, the South Korean government established an 11% target of new and renewable energy sources in total primary energy supply by 2030[6]. The seriousness of the Korean government is demonstrated by an investment of over 600 billion Korean Won (KRW) in research, development and demonstration in 2010[3].

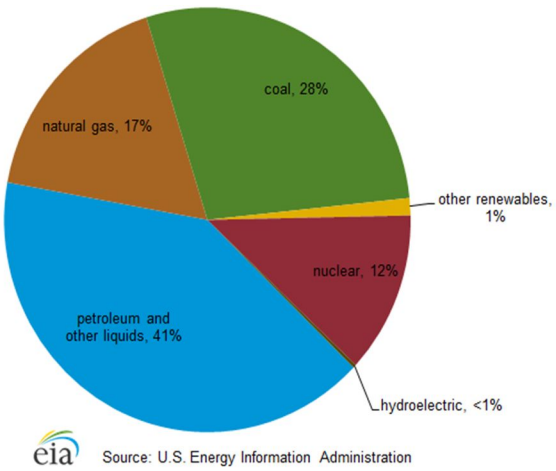

Figure 3 Distribution of fuel types in South Korea's total primary energy consumption 2012[3]

2 THEORY

2.1 SOLAR ENERGY

One of the before mentioned green energy sources is based on harvesting light from the sun, therefore called solar energy. Many methods of converting solar radiation to applicable forms of energy have been developed over the years from solar heating, and solar photovoltaic to artificial photosynthesis.

In this thesis the focus lies on organic photovoltaic devices (OPV), which convert solar radiation into usable direct current (DC) electricity by utilizing unique properties of organic semiconductors.

2.2 ORGANIC SEMICONDUCTORS

Organic semiconductors are carbon-based materials possessing semiconductor characteristics. In semiconductors free charge carriers can be created by thermal, optical or chemical processes. The bonding mechanism of atoms within the organic semiconductor molecule is based on conjugated π-bonds, while molecules are bonded by van der Waals forces[7].

Compared to inorganic semiconductor materials, flexibility, light weight and low temperature processing allow for cheap and large area application of organic semiconductors. Band structure of organic semiconductors can be treated similarly as inorganic semiconductors. The valence band is normally filled with electrons and the conduction band is normally free of electrons.

In organic semiconductors, the Highest Occupied Molecular Orbital (HOMO) and the Lowest Unoccupied Molecular Orbital (LUMO) are analogs to the valence band and conduction band respectively. Organic molecules and molecular crystals with

conjugated π-electron systems possess electronic excitation energies in the range of only a few *eV* (electron volt) and absorb or luminesce in the visible, the near infrared, or the near ultraviolet spectral regions. The electronic excitation energies of this absorption shift towards lower energies with increasing length of the conjugated system[8]. The primary photogenerated state arising from light absorption in organic electronic materials is an exciton, a quasiparticle consisting of an electron in the LUMO and a hole in the HOMO.

As the van der Waals interactions between molecules are much weaker than the bonds within the molecules, the so-called Frenkel excitons in organic materials are more localized and much less extensive than the excitons in crystalline inorganic semiconductors (known as Mott-Wannier excitons). Additionally, migration of excitons in organic materials occurs by a relatively slow process of hopping between localized sites, leading to low carrier mobilities. Nonetheless, extensive research steadily improves π-conjugated polymers[9], and organic semiconductors will most likely become the next-generation of electronic material.

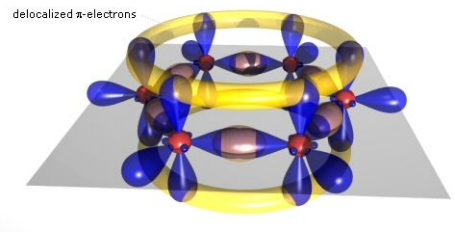

Figure 5 Scheme of a benzene ring with delocalized π-electrons (yellow)[62]

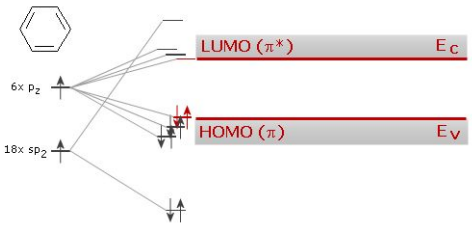

Figure 4 Energy structure of a benzene ring with HOMO and LUMO levels [62]

2.3 WORKING PRINCIPLES OF SOLAR CELLS

The basic operation principles of organic solar cells based on donor-acceptor materials can be broken down into individual steps for simplification. Photons with energies equal or greater than the HOMO-LUMO gap are absorbed by the organic molecular materials. After light absorption takes place in the active layer, an exciton is generated. But the lifetime of excitons (τ_{exc}) is very short due to various radiative and non-radiative decay processes. With the low mobility in organic materials, exciton diffusion length (L_{exc}) is limited to ~10 nm before the exciton recombines.

$L_{exc} = \sqrt{D_{exc} \cdot \tau_{exc}}$; With D_{exc} = diffusion coefficient of excitons

To prevent recombination, donor and acceptor materials are mixed to establish a so called bulk-heterojunction. In this interpenetrating network a donor-acceptor interface can be reached from any point in the active layer within distances $d < L_{exc}$. Excitons diffuse to the interface of the donor and acceptor material and the built-in

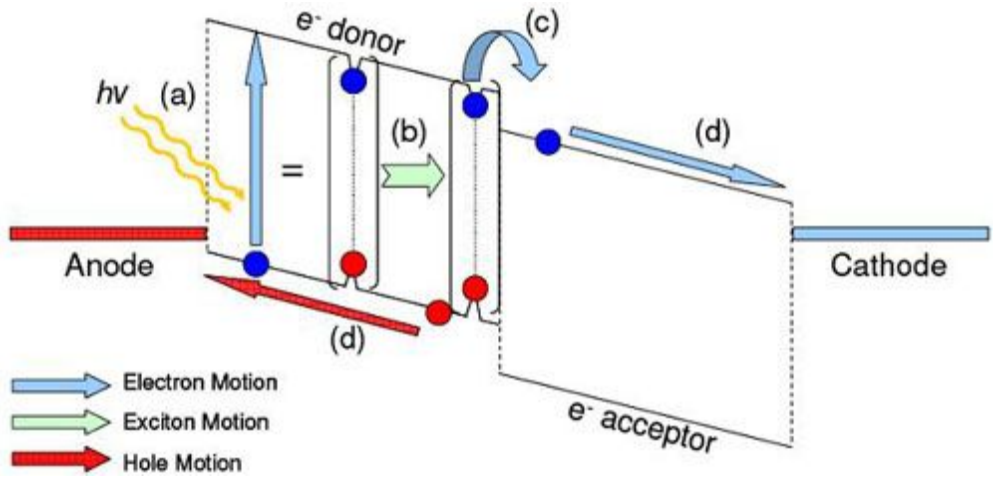

Figure 6 Simplified operation principle of donor-acceptor solar cell: (a) Photons are absorbed in the active layer (b) excitons diffuse to the donor-acceptor interface (c) excition is separated in free electron and hole (d) transport to respective electrode

electrical potential separates the electron-hole pair into free electrons and holes. Charges are transported and subsequently collected at the electrodes, where they are conducted to an external electric circuit[10].

2.4 Current-Voltage (I-V) Characteristics of Solar Cells

Typically, current-voltage characteristics, known as IV curve, are used to determine performance and electrical characteristics of photovoltaic devices. An exemplary current-voltage characteristic of a solar cell under dark and illuminated conditions is shown in Figure 7 Current-Voltage characteristic under dark and illuminated conditions. Short circuit current I_{SC} flows with zero external resistance (V=0) and is the maximum current delivered by the solar cell at any illumination level. Similarly, the open circuit voltage, V_{OC}, is the potential that develops across the solar cell when the external load resistance is very large and no current flows.

The Fill factor, *FF*, is defined as the ratio of the maximum power from the solar cell to the product of V_{oc} and I_{sc}, and is often used to estimate the power that a cell can provide with an optimal load under given conditions. The fill factor is defined as

$$FF = \frac{I_m \times V_m}{I_{SC} \times V_{OC}} \qquad (1)$$

with I_m and V_m representing current and voltage at maximum power output. The FF is also graphically measured as the ratio of the area of the I-V curve and the largest rectangle, which fits in the curve (Figure 7 Current-Voltage characteristic under

dark and illuminated conditions). The efficiency of a solar cell, which is defined as the fraction of incident power converted to electricity, is the most commonly used parameter to show the performance of solar cells. The power conversion efficiency η is given by

$$\eta = \frac{V_{OC} \times I_{SC} \times FF}{P_{in}} \qquad (2)$$

where P_{in} is the incident power. Because of the wavelength and light intensity dependence of the photovoltaic response, the efficiency should be measured under standard test conditions. The standard current-voltage characteristics include the measurement of current and voltage under simulated (100 mW cm^{-2}, AM 1.5G) solar spectrum conditions.

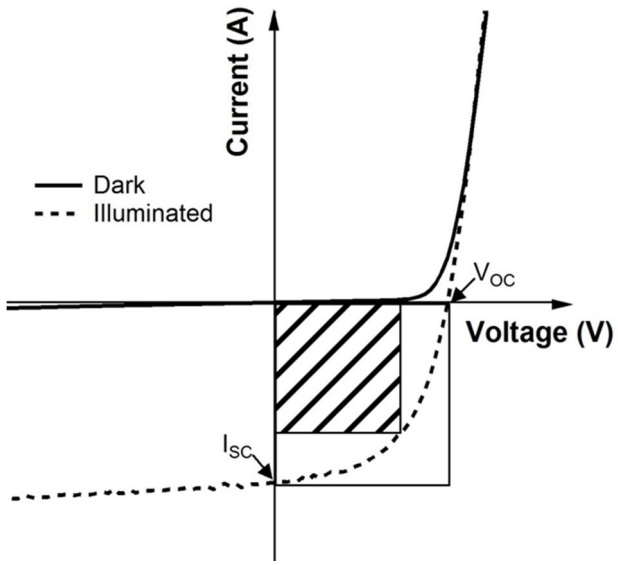

Figure 7 Current-Voltage characteristic under dark and illuminated conditions [11]

3 ELECTRODES

Electrodes are essential components in the fabrication of any electrical device. The same is valid for organic optoelectronics: an electrode provides the contact of the external circuit with the photoactive device. In case of solar cells electrodes transport charges, which are generated in the active layer materials to the external circuit. In the opposite way, electrodes in light emitting diodes (LED) transport the charges, which are provided by the external circuit to the active layer to generate photons. The term 'electrode' is not limited to one material. Composites of organic and inorganic materials can be combined and labeled as electrode. In that sense, charge transport or blocking layers and the connecting material are often defined as electrode.

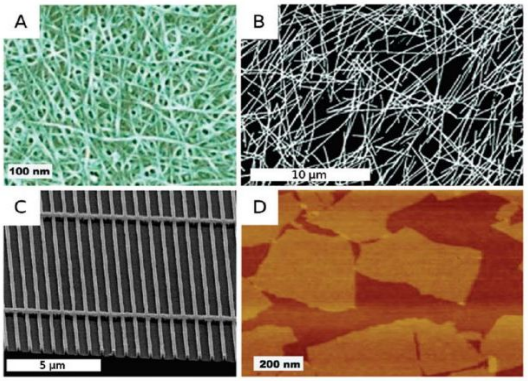

Figure 8 materials for transparent and conductive electrodes. (A) carbon nanotube film (B)silver nanowire network film (C) Au nanowire grating (D) graphene flakes [63]

Electrodes have to fulfill certain requirements[12] to be used in optoelectronic devices:

1. High conductivity

   In order to transport charges effectively, electrodes have to possess low electrical resistance to minimize losses.

2. Chemical and electrochemical stability

   Materials used as electrodes should not contribute to degradation of connected active material in the device. In an ideal case, electrodes provide additional protection as barriers from external effects, like oxidation or moisture.

3. Transparency

   As light harvesting in solar cells takes place inside the device, at least one electrode has to be transparent. Therefore, in transparent devices both sides have to permit light flux. In order to archive high performance solar cells, electrodes should have high transparency in the wavelength spectrum in which the device operates. So both, absorption and reflectivity of the transparent electrode, should be low.

The choice of electrode material depends largely on the device requirements: whether the electrode contact is used in a basic Schottky-type cell with a single organic photoconductive material, or in a bulk-heterojunction device with ohmic contacts between electrode and active layers. For achieving an ohmic contact with the smallest possible barrier at the electrode, a high work function material for the hole-collecting contact (anode) and a low work function material for the electron-collecting contact (cathode) is used.

So, besides its electrical resistance, the work function of the electrode material plays a critical role. It is reported[13] that in bulk-heterojunction solar cells the V_{OC} is governed by the LUMO and HOMO levels of the acceptor and donor, respectively, which pin the Fermi levels of the cathode and anode. The band bending, created by accumulated charges at an ohmic contact, produces a considerable loss in V_{OC} of 0.2 V at room temperature. In case of ohmic contacts at both electrodes a voltage

loss of 0.38 V in V_{OC} has been observed. In experiments [14] with different materials, it has been discovered that an increase in workfunction of the metal top electrode leads to a reduction of the open-circuit voltage, short-circuit current, and power conversion efficiency of organic bulk-heterojunction solar cells. Therefore the choice of a suitable electrode material will maximize the V_{OC} and increase device efficiency.

Nearly all organic solar cells fabricated at the moment use a conductive metal layer (e.g. Al, Ag, or Au) as rear electrode, and a conductive transparent metal oxide film (e.g. ITO (In_2O_3:Sn) as front electrode. But especially the use of ITO stands in stark contrast to the often mentioned advantages of organic solar cells as being a cheap and easy to manufacture alternative to silicon based solar cells.

The good electrical properties of ITO with a sheet resistance (R_S) ~5-10 Ω/□ and transmittance (*T)* of ~90% justify its frequent use in research oriented manufacturing. But Indium is a very scarce and expensive material with high processing costs, which account for 29% of final module costs for commercially viable organic solar cells [15]. The high processing temperatures needed for producing high quality ITO films limit its application as many organic materials cannot withstand these temperatures.

Another disadvantage of ITO is its brittleness on PET substrates. Especially with the increasing popularity of flexible electronics in OLED and OPV production the demand for a more robust material is rising.

This analysis motivates the search for alternatives for ITO as electrode material in organic electronics[16]. Among the suggested materials to replace ITO, the most promising are high conductive polymers[17], carbon nanotubes [18] , graphene [19], nanowires [20], and metal grids[21]. Challenges that have to be overcome

include-but are not limited to- high transmittance, low sheet resistance, high flexibility, good adhesion to substrate, low cost material and compatibility to large area manufacturing processes.

3.1 Silver Nanowire Networks

Metals have long been used in electronics due to their high electrical conductivity. With Silver (Ag), Copper (Cu), Gold (Au) and Aluminium (Al) being among the best conducting, these materials have been used the most (Table 1). Bulk metals show high reflectivity in the visible spectrum, so their use in transparent electrodes was not suitable.

This was until manufacturing technologies and precise control over layer thickness deposition advanced to a level where ultra-thin metal films could be fabricated.

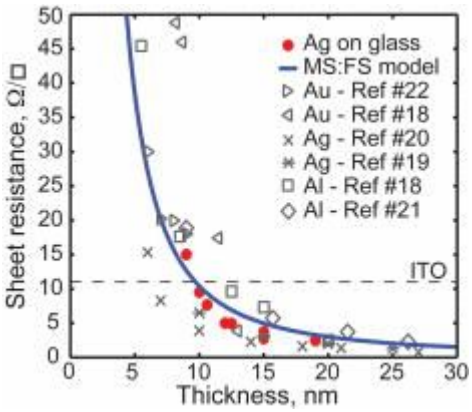

Figure 9 Experimentally determined sheet resistance vs metal films thickness for Ag, Al, and Au, compared to nominal sheet resistance of ITO [23].

Metal	σ (S/m) at 20 °C
Silver	6.30×10^{7}
Copper	5.96×10^{7}
Gold	4.10×10^{7}
Aluminium	3.5×10^{7}

Table 1 Metal conductivity at room temperature [22]

With decreasing layer thickness down to tens of nanometers, metals become transparent[23]. As predicted in the Fuchs-Sondheimer theory, thinner films

generally exhibit higher resistivity due to electron scattering from the surface and grain boundaries[24], which make them less ideal in use for transparent electrodes. Therefore, research moved to patterned metal grids instead of continuous metal sheets. The area between the metal grid lines is 100% transparent and increases the overall transparency of the film.

A tradeoff with higher sheet resistance can be compensated by increasing diameter or quantity of metal grid lines at the cost of change in layer morphology. Depending on the device requirements an individual tuning of these parameters has to be accounted for.

Processes used to generate metal grids range from nanoimprint lithography[25] to roll-to-roll compatible screen printing[26], but fabrication of patterned metal grids still proves to be very difficult, and slow in process, as well as combined with high costs.

The recent introduction of random metal nanowires networks[27][28] combines the advantages of patterned metal films with low cost solution processing.

3.2 Synthesis of Silver Nanowires

Large-scale synthesis of silver nanowires was first demonstrated[29] by using platinum nanoparticles as seeds for the heterogeneous nucleation and growth of silver, formed by reducing $AgNO_3$ with the polyol ethylene glycol. Silver nanowires with diameters in the range of 30-40 nm and lengths up to 50µm were synthesized. In recent years the processes have been much improved and lead to higher quality in terms of length and diameter distribution, as well as material purity[30][31]. Other methods for forming silver nanowires include hydrothermal, microwave-assisted[32] or electrochemical techniques, but due to its simple and fast[30]

approach the polyol method is the most suitable for mass production. The growth mechanism cannot be exactly explained yet, but progress is made[33]:

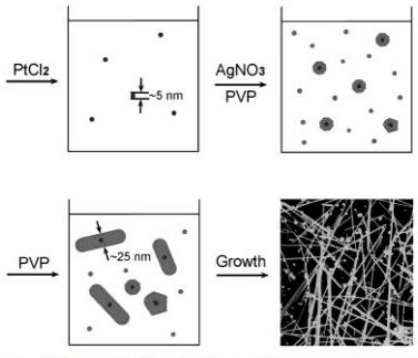

Figure 10 Schematic illustration of the experimental procedure that generates silver nanowires through a Pt-seeded polyol process [29]

Ethylene glycol reduces the metal precursor silver nitrate ($AgNO_3$) in the presence of a nucleating agent and polyvinyl pyrrolidone (PVP). PVP is used as capping agent to control the growth rates of different surfaces of silver nanoparticles. Ethylene glycol as a reducer is chosen based on its ability to solvate both $AgNO_3$ and PVP, combined with its stability at high temperatures. In the first step of the process ethylene glycol reduces Ag+ ions in Ag atoms, thereby inducing silver crystal formation and subsequently growth of silver nanostructures.

The synthesis of AgNWs has therefore three distinct steps:

1.) nucleation
2.) evolution of nuclei into seeds
3.) growth of seeds into nanocrystals.

In these steps atomic addition and aggregate formation are governed by mechanisms of diffusion and surface energy minimization. The seed structures have an important role in the shape evolution of metal nanocrystals and therefore in the resulting materials. According to *Xia et al*[33] the nanowires are derived from multiple-twinned particles. These particles provide the most thermodynamically

stable seed, as it is bound almost entirely by lower energy {111} facets. This makes it the most abundant seed, but also the most reactive because of the presence of twin defects.

The crystalline defects where the cores are exposed, provide active sites for growing the nanowires along their longitudinal axes, while the less-strained side surfaces of the nanowires, bound by {100} facets, have lower reactivity towards the deposition of silver atoms (Figure 11). Once the pentagonal rod is formed, PVP plays a key role in the growth mechanism: it reacts preferentially with the {100} facets of the silver nanoparticles, through interactions between surface silver atoms and the oxygen atoms of the PVP carboxyl groups [34]. Processing temperature, injection rate, molar ratio of PVP to silver nitrate, sodium chloride amount, and stirring rate - all play an important role and for some of them tiny changes can lead to dramatic alterations of size and shape of the nanoparticles.

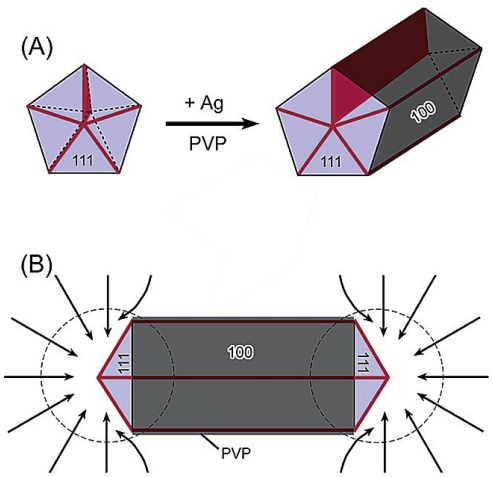

Figure 11 Schematic illustration of the mechanism proposed to account for the growth of silver nanowires (A) Evolution of a nanorod from a multiply twinned nanoparticle of silver under the confinement of five twin planes and with the assistance of PVP (B) Diffusion of silver atoms toward the two ends of a nanorod, with the side surfaces completely passivated by PVP [33]

As the length to diameter ratio, called Aspect Ratio (AR), plays a key role in charge conducting properties, emphasis lies in the synthesis of long and thin nanowires. Recently nanowires with 300 µm length and diameter of less than 150 nm were attained by a successive multistep growth process[35]. After synthesis the

nanowires are purified, filtered and diluted in numerous solvents like isopropyl alcohol (IPA), deionized water or ethanol.

3.3 Effect of Nanowire Length on Transparency and Conductivity

How big the effect of nanowire length on electrical properties is, was shown in Monte Carlo simulations[36] for widthless sticks in two dimensions. These simulations show that for sticks with a given length L, the critical number density N_c of sticks required for percolation is given by

$$N_c L^2 = 5.71 \qquad (3)$$

This equation indicates that longer nanowires will make for qualitatively better transparent conducting films, as doubling the length of the nanowires decreases the number density of nanowires required for percolation by a factor of four. If more nanowires are added to a film that has just achieved percolation, more connections will be made with nanowires that were not touching the conducting path, and the conductivity of the network will increase. When the number density of nanowires (N) is close to but sufficiently above N_c, the relationship between the conductivity of the film and the number density of nanowires is given by

$$\sigma \propto (N - N_c)^t \qquad (4)$$

Here σ can be taken as the sheet conductance of the film (the inverse of the sheet resistance), and t is the conductivity exponent. The conductivity exponent

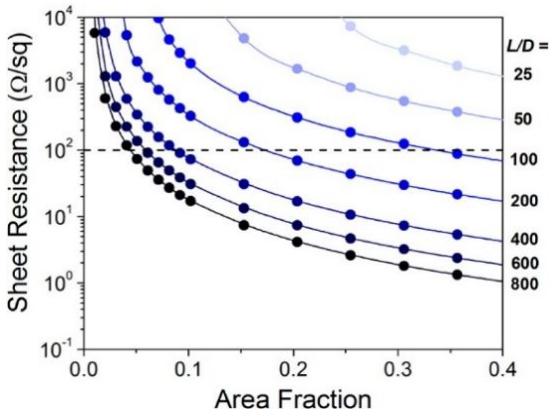

Figure 12 Simulated sheet resistance (R_s) for silver nanowire thin films as a function of the area fraction (AF) for various L/D values [38]

increases with $R_j/R_{st,}$ because adding an additional wire to a well-connected network will have a bigger impact, if it shortcuts many highly resistive junctions. The conductivity exponent based on an approximate film thickness for silver nanowires resulted in a high value of 1.9. In simulations[37] R_j = 2kOhm was found to be the best fit to experimental data. This rather high resistance of a single junction compared to the film sheet resistance shows how important the wire connectivity is. Based on R_j quantitative predictions of AgNw films prepared by comparable methods as a function of areal density, nanowire length and diameter, size dispersity, and nanowire orientation can be made.

Combining the findings on R_j and effect of nanowire length in form of area fraction as

$$AF = NLD \qquad (5)$$

the dependence of sheet resistance on nanowire aspect ratio and area fraction has been simulated by *Winey et al.*[38] (Figure 12).

The strong relation of R_S to aspect-ratio highlights the pursuit of improved synthetic methods to produce ultra-high-aspect-ratio nanowires to optimize sheet resistance.

3.4 TRANSPARENCY TO SHEET RESISTANCE

Wire density is a crucial parameter in the optical and electrical properties of the network. With higher density networks transparency decreases and it is shown[39] that an increasing number of wires lower the sheet resistance. Only recently theoretical models have been formed that adequately simulate the attained experimental data[37]. Models based on bulk like behavior regarding conductivity and transparency are not sufficient in describing the properties of random

networks. In percolation theory, the percolation threshold of a component has to be overcome to form a connected system, which in case of nanowires allows charge flow. Increasing the density of nanowires above the percolation threshold results in conduction pathways through the network that are in parallel, hence as the number of conduction paths increase, the resistance decreases. The necessity of treating silver nanowire networks in the percolative regime and not bulk-like can be seen in the fit of both models to experimental data in Figure 13.

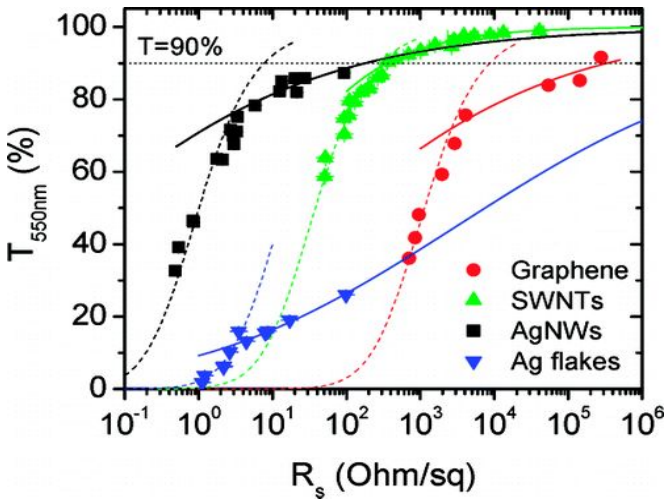

Figure 13 Transmittance (550 nm) plotted as a function of sheet resistance for thin films prepared from graphene, single-walled carbon nanotubes, silver nanowires, and silver flakes. The dashed lines represent fits to the bulk regime , while the solid lines represent fits to the percolative regime [64]

Transparent conductors for high performance applications must display both, a low sheet resistance ($R_s \leq 100\ \Omega/\square$) and high optical transparency ($T > 90\%$). Optimizing these two properties simultaneously is challenging as better transmittance requires reducing the area fraction of nanowires, while decreasing area fraction increases the sheet resistance. *Bergin et al*[40] studied the optical properties of silver nanowire films via experiments and FDTD simulations, reporting a linear

relationship between network transmittance and area coverage of nanowires for a given diameter. Moreover, the optical properties were determined to be independent of the nanowire length. An empirical relationship between the area fraction (*AF*) and the optical transmittance at λ = 550 nm could be established:

$$\%T = 100 - a_1 AF \qquad (6)$$

Where a_1 is a fitting parameter that accounts for the diameter and wavelength-dependent optical properties of the nanowires. For nanowires with D_{nw} ~ 40 nm, Bergin validated a_1 = 87. By combining this empirical expression and simulated R_s values using R_j = 2 kΩ, both the *%T* and R_s dependence on nanowire length and area fraction were predicted[37](Figure 14). The figure shows that high *AR* is advantageous for increasing *%T* at a fixed R_s, but intermediate *AF* are needed to produce films suitable for high performance application.

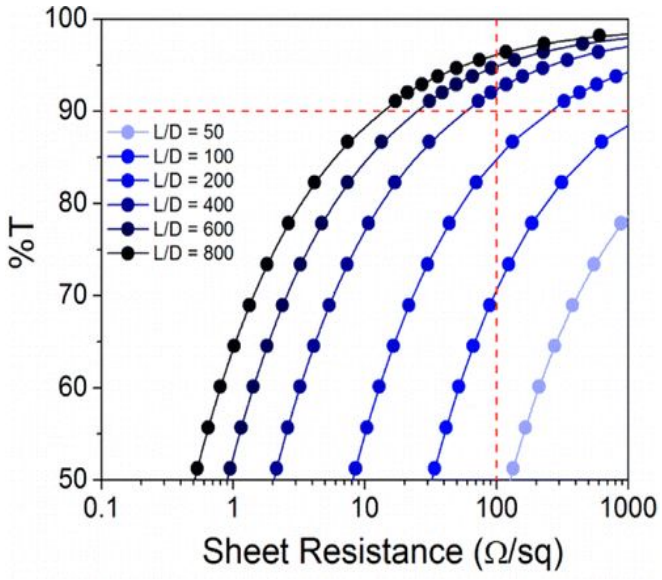

Figure 14 Calculated transmittance vs simulated sheet resistance for silver nanowire films for L/D ranging between 50 and 800 [38]

3.5 Deposition of Silver Nanowires

Fabrication of transparent electrodes has to be cost-efficient, low temperature and reliable. To fulfill these requirements different techniques are used to fabricate high performance silver nanowire networks. Solution based methods such as spray coating, drop casting, rod coating or spin coating are simple and successfully used in the production of electrodes[41][42]. Other methods involve electrospinning [43] or lamination[21][44]. The choice of method also has an effect on uniformity and therefore quality of the networks and has to be individually optimized. Depending on device application different requirements apply for acceptable morphology, environmental stability and contact resistance.

For the use in organic photovoltaics, transparency plays an important role. The use of spin coating gives good control over density distribution of nanowires by adjusting spin speed or solvent ratio[45]. Working principle of spin coating is shown in Figure 16 and how film thickness relates to spin speed or time is shown in Figure 15.In the experimental section of this work, individual optimization for various substrates is shown.

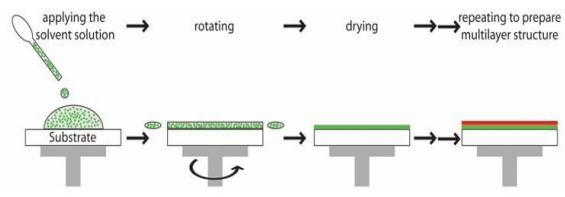

Figure 16 Subsequent steps of the spin-coating process

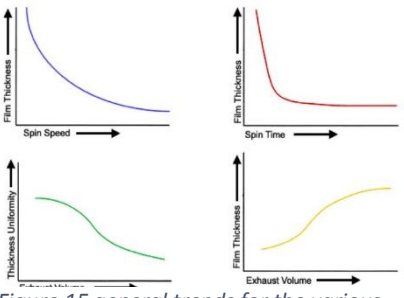

Figure 15 general trends for the various process parameters [65]

3.6 POST-PROCESSING OF SILVER NANOWIRES

As shown previously, a crucial parameter in forming electrical properties of metal networks is junction resistance. R_j is determined by the nature of the junction: this is dependent on how the nanowires are grown, purified, and deposited. Due to the possible surfactant coating of polyvinylpyr- rolidone (PVP) on the surface of AgNWs and the loose contact between AgNWs, extra treatments are often required to fuse the crossed AgNWs together. Different methods of modifying junction resistance have been studied in literature and been applied. Thermal annealing[46], high pressure[47], electrical annealing, optical sintering and encapsulation[48] have all been shown to reduce the resistance of the network. Even graphene oxide nanosheets were used as over-coating layer for metal junctions[49].

An additional benefit of welding the nanowire junctions is the flattening of the layer morphology. After initial deposition nanowires lie on top of each other in staples and create layers with thicknesses multiples of the nanowire diameter. Indeed a mildly roughened (<10nm) or structured surface can enhance the performance[50], but in case of nanowires the roughness is too big and leads to short-circuited devices. So above mentioned methods to fuse the junctions like thermal annealing or applying high pressure help to establish a smoother surface, which is necessary for successive layers.

In case nanowires are used as top electrode, the underlying layers should not be harmed by the post-processing. Here a light-induced plasmonic nanowelding technique[51] to assemble metallic nanowires into large interconnected networks resembles a possibility. The small gaps that form naturally at nanowire junctions enable effective light concentration and heating at the point where the wires need to be joined together. The extreme sensitivity of the heating efficiency on the junction geometry causes the welding process to self-limit when a physical

connection between the wires is made. The localized nature of the heating

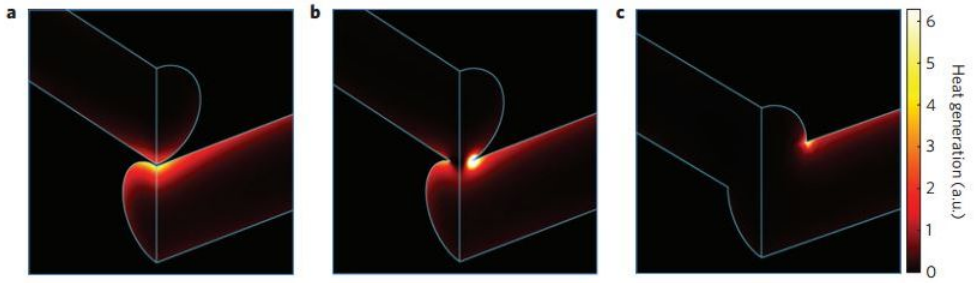

Figure 17 Heat generation profile for a nanowire junction while illuminating with polarized light with 800 nm wavelength [51]

prevents damage to substrates, such as plastics and polymer solar cells.

Post-processing steps are also used to create strong adhesion between AgNWs and the substrate to obtain stable and robust AgNW films. Substrate surface modification with UV-light, applying strong conformal pressure or encapsulation can enhance adhesion. Another strategy is embedding metal nanowires in a material matrix. Either to enhance the properties of the host-matrix[52] or as mentioned above, improve adhesion and conducting properties of nanowires by embedding them in e.g. conductive metal oxide nanoparticles[53]. Embedding nanowires in an environmental stable material can help prevent metal oxidation[54] and increase thermal stability up to 375°C[55], allowing high temperature application.

3.7 ELECTRODE PATTERNING

Forming well defined patterns of the electrode material allows better performance characterization and device integration. Dividing the electrode layer in equally sized sections minimizes the effect of impurities or defects in measurements. Especially with rough morphologies occurring in nanowire layers shunt resistance (R_{sh}), which provides an alternate current path for the light-generated current, causes power losses in solar cells.

The use of conventional photoresist processing used in inorganic device patterning is difficult, as many organic materials degrade when exposed to solvents or aqueous chemicals. Given the low electrical conductivity of most organic thin films, electrode patterning alone is generally sufficient to define the device. In case of nanowire deposition by ink-jet printing, stamp or lift-off methods patterning is not an issue. For solution-based processes it is more of a challenge as the whole substrate is covered in one interconnected network. Cutting[56] the nanowire networks by hand is a viable option in laboratory environments but not suitable for roll-to-roll manufacturing. Depending on the position of the nanowires on top or bottom of the cell, certain areas should not be covered by solution.

To achieve this, two methods are presented in this work: first a rudimentary way in which copper tape is applied to the substrate before spin-coating the nanowires as bottom electrode and removing it after all, but the upper electrode layer is deposited, leaving the substrate blank in this area.

The second method involves thermal evaporation of silicon dioxide (SiO_2) as dielectric on top of the nanowire network. Samples with AgNWs and optional

charge-transport layer are spin-coated on the substrate. A shadow mask is used to define the electrode areas and shield them from thermal evaporated SiO_2. 200nm SiO_2 is deposited in the dark blue area (Figure 18 Patterning Mask for AgNW layers. Light blue area is the masked area and dark blue is covered with SiO2) to insulate the area and protect the device from being short-circuited due to nanowires breaking the active layer surface. The nanowire network is intentionally left intact to retain the good conducting properties of the film. Active area of the device is defined by the overlap of the light blue area with the Aluminium top electrode (grey).

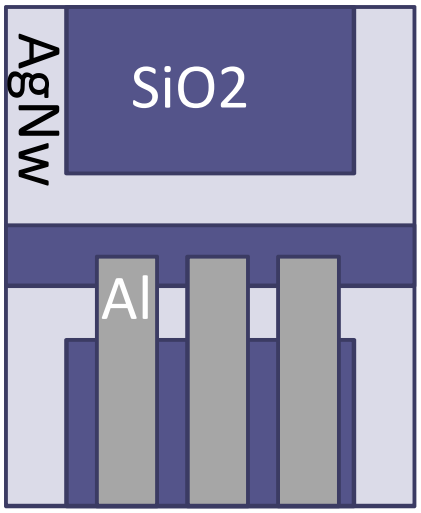

Figure 18 Patterning Mask for AgNW layers. Light blue area is the masked area and dark blue is covered with SiO2

4 EXPERIMENTAL SECTION

4.1 MEASUREMENTS

The transmission spectra of films were measured on a PerkinElmer Lambda 35 UV-Vis spectrophotometer. AFM images were obtained with a Digital Instruments Nanoscope IIIA in tapping mode. The current density-voltage (J-V) characteristics of the devices were measured with a source measurement unit (Keithley SMU237). The device performances were characterized under AM 1.5G condition with an illumination intensity of 100 mW cm^{-2} using a solar simulator (Newport 91160A).

4.2 ELECTRODE FABRICATION

4.2.1 Optimization of Nanowire Density

The silver nanowires are purchased from Tokusen Kogyo Japan[57] and have an average diameter of 50nm and an average length of 15µm. So the nanowires have an aspect ratio (*AR*) of ~300, which predicts a good but not excellent performance range (p.15). IPA is chosen as solvent because of its proven compatibility to PEDOT:

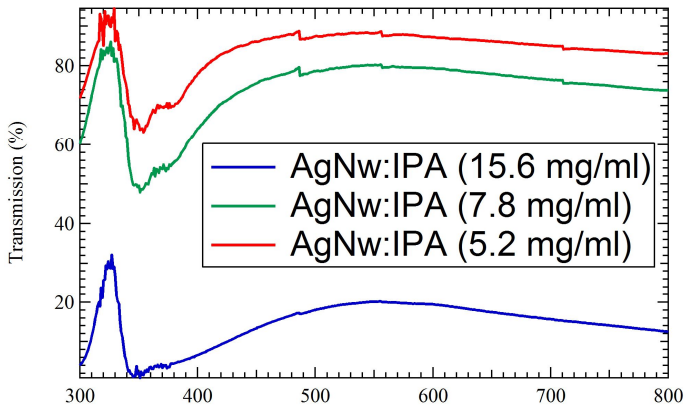

Figure 19 Transmission spectrum of AgNW films with various dilution ratios; samples are prepared at constant spin speed

PSS and other often used charge transport materials. The nanowires have a 2wt% in the purchased solution, which equals to about 15.6 mg/mL. Before spin-coating the glass substrates are cleaned in Acetone, IPA and deionized water for 20 min each. After drying in an oven at 120°C for at least 3h, substrates are radiated with UV-light for 10 min.

The initial nanowire concentration proved to be too high to achieve uniform films: the nanowires agglomerate and form spots on the substrate. This can be avoided by diluting the solution with additional IPA. In search for the best concentration, various dilution ratios are mixed and analyzed.

Figure 19 shows the dependence of transmission on dilution ratio. As theory predicts, an increasing area fraction covered by nanowires leads to a decline in light transmission. For this experiment the spin-speed of the coating process is kept constant to allow a comparison of the mixtures. To relate this transmission data to electrical performance, R_S is measured (Table 2).

Table 2 Transmission and sheet resistance of various AgNW concentrations

Mixing ratio	R_s (Ω/□)	Transmission@550nm (%)
AgNw:IPA (15.6 mg/ml)	1.34	20.07
AgNw:IPA (7.8 mg/ml)	7.96	80.13
AgNw:IPA (5.2 mg/ml)	12.29	88.27

Additionally AFM imaging is utilized to get a better understanding of the network's formation process.

AFM images (Figure 20) indicate the structures formed by the coating process. The above mentioned spots on the substrate with the undiluted mixture are caused by clustered nanowires and cause unfavorable optical and morphological properties.

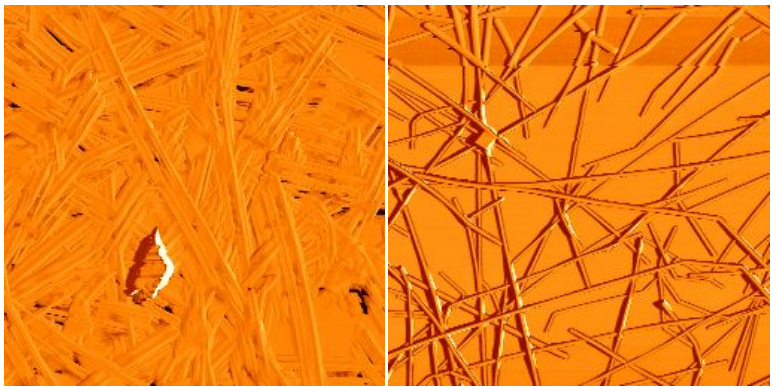

Figure 20 AFM images of AgNW:IPA solution; (left) 15.6 mg/ml (right) 5.2 mg/ml

In contrast, the AgNW:IPA (5.2 mg/ml) mixture forms a proper network.

4.2.2 Optimization of Spin-speed

In spin-coating the spin-speed is next to the solution composition a major factor in controlling film properties. As both parameters are interdependent, the previously established dilution ratio is fixed in the experiments to balance transmission and sheet resistance of the established networks. Nanowire films generated with spin-speeds from 500 rpm to 3000 rpm are fabricated and compared. The experimental data (Figure 21 Dependence of sheet resistance on spin-speed; effect of annealing on sheet resistance) confirms the theoretical model which predicts lower sheet resistance with increasing area fraction (Chapter 3.3).

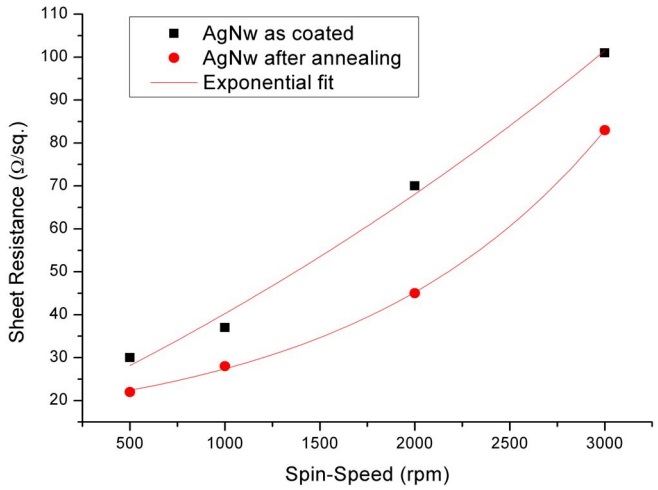

Figure 21 Dependence of sheet resistance on spin-speed; effect of annealing on sheet resistance

4.2.3 Post-processing of Nanowire Networks

The so established nanowire networks already show good electrical properties with sheet resistance of 30-120 Ω/□ without any post-treatment. To properly connect the nanowire junctions and to remove PVP and solvent residue, thermal annealing is performed on a hotplate for 10 min. at 150°C. This decreases the R_S by ~25% for the sample fabricated at 1000 rpm and shows a transmittance of 90.94% at 550nm.

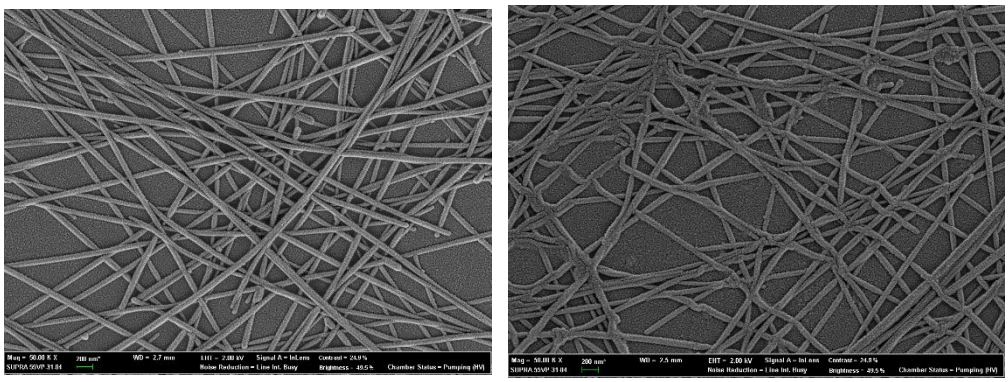

Figure 22 SEM images before (left) and after thermal annealing (right)

The effect of annealing can be seen in SEM images taken before and after processing. Untreated nanowires are straight and stiff like uncooked spaghetti, whereas the annealed nanowires are bent on nanowire crossings (Figure 22).This leads to an increased contact area and flatter morphology, especially on junctions with multiple wires.

Figure 23 demonstrates how sensitive nanowires are to slightly higher temperatures (~170°C). Nanowire crossings are melting and individual wires break up under thermal induced stress. This fact limits device fabrication after nanowire deposition to low temperature range (<150°C), except if special shielding materials are implemented.

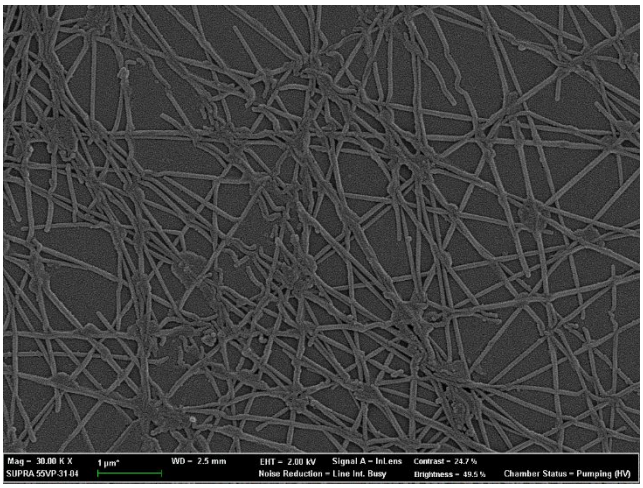

Figure 23 SEM images after higher temperature

4.2.4 Experiments with Spin coating on Plastic Substrates

Besides glass, Polyethersulfone (PES) is used as substrate for experiments. PES is a thermoplastic polymer with high durability and flexibility, so it can be used in bendable electronics. The same process as for glass substrates is used to create the nanowire networks. UV-curing of the substrate before spin-coating decreases adhesion and is therefore omitted. PES withstands the thermal treatment at 150°C without any signs of degradation. Measurements of R_s produced better values in the center of the substrate. This is attributed to a height gradient caused by the vacuum suction which holds the substrate to the spin-coating head. The generated dip leads to higher solution concentration and therefore denser nanowire network, with a slightly visible reduced light transmission. This should be avoided by using a more stiff holding apparatus for plastic substrates.

Adhesion of the nanowire network to the PES substrate is checked by performing a scotch tape test. Samples are prepared and 3M Scotch tape is attached firmly and

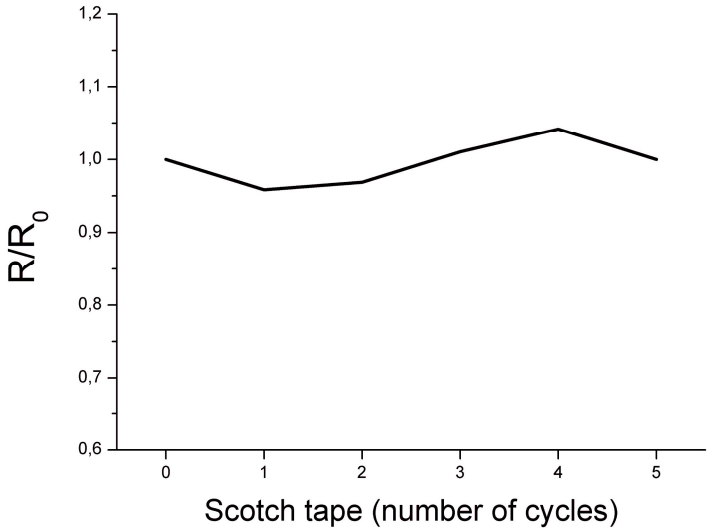

Figure 24 Adhesion of AgNW film to the substrate is tested with scotch tape

removed. The tape is replaced and the process is repeated.

R_s is measured to examine changes in performance (Figure 24 Adhesion of AgNW film to the substrate is tested with scotch tape). The data is acquired with two probe electrical measurements, performed by the direct contact of alligator clips on the flexible substrates.

Except for a small deviation caused by the measurement method, resistance does not change relative to initial values, even after repeating the test five times. This attests firm adhesion to the substrate and good mechanical properties. Further processing steps can be taken without risking damage to the nanowire network by moderate physical stress.

4.2.5 Influence of Bending

The use of plastic substrates is motivated mostly by their flexibility. Consequently materials used in devices based on plastic substrates should possess similar properties.

To investigate the impact of flexion on electrode performance, we designed a bending benchmark test: samples undergo 180° bending angle at a 3mm bending radius. This is repeated numerous times while R_s is measured to visualize the impact on performance. Silver nanowires on PES substrate with initial $R_s \approx 20\ \Omega/cm$ are fabricated and compared to ITO coated PET films, purchased from Xin Yan

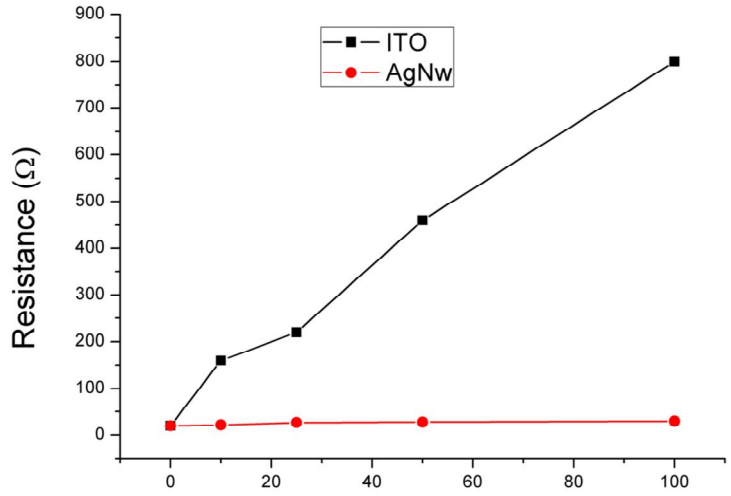

Figure 25 Influence of bending on sheet resistance of AgNW and ITO samples

Technology[58] with reported $R_s \approx 15\ \Omega/\square$ (measured $R_s \approx 20\ \Omega/cm$).

ITO substrates already show a nearly tenfold increase in R_s after 10 bending cycles. The brittle ITO layer easily cracks, leading to decrease in conductivity and as a result drop in the device performance. AgNWs clearly demonstrate their high flexibility with constant electrical properties even after 100 cycles. Single nanowires bend easily and due to their random orientation mechanical stress is reduced depending on their alignment with the bending. A sufficient dense network of wires still allows good percolation even with isolated broken wires. This test states the potential of silver nanowires for implementation in flexible electronics.

4.2.6 Time-dependent Performance Development under Air Exposure

Metals tend to oxidize under air exposure and the formation of metal oxides leads to changes in electrical and optical properties. In case of an optimized material system oxidation decreases device performance.

Samples coated in vacuum compared with samples coated in air show no difference in performance. In order to observe the behavior of silver nanowire films under a longer period of air exposure, samples are stored in ambient air environment and measured over a period of nine days.

As shown in Figure 26 degradation varies depending on the initial properties of the film. Samples with high nanowire density show a more stable performance compared with lower density networks. Sparse networks rely more heavily on single conducting paths. Omission of individual wires due to oxidation effects has a higher impact on conductivity. Altogether the films demonstrate high stability under environmental conditions, which allows their use as material for top electrodes in electronic devices.

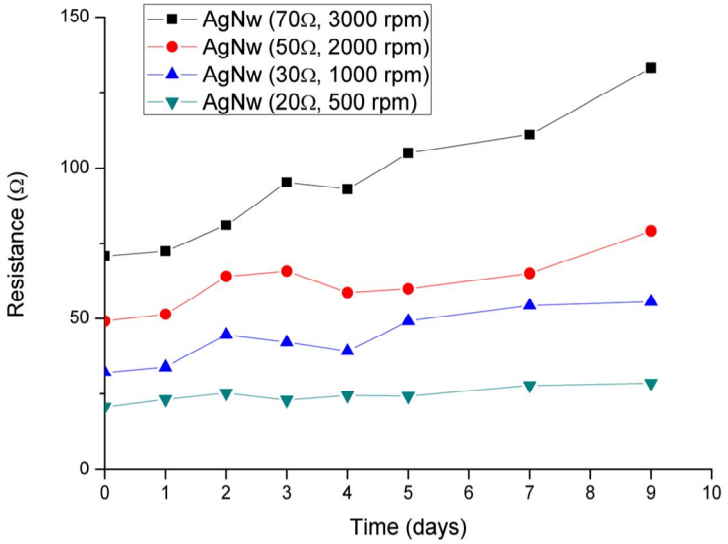

Figure 26 Time evolution of sheet resistance of AgNw films over nine days air exposure

4.2.7 Implementation of Copper Nanowires

An attempt was made to fabricate networks based on copper nanowires. Copper nanowires are even more cost effective than silver nanowires with similar physical properties[59]. Dry nanowires with 100 nm diameter and 5 µm length were purchased from CNVISION CO.[60] and mixed with various solvents (IPA, DI water, ethanol, chlorobenzene). None of the mixtures could produce a uniform film similar to the silver nanowires networks. Therefore copper nanowires were implemented stepwise into silver nanowire solution to observe changes in electrical and optical characteristics. Ratios of copper nanowires from 0-25wt% were mixed and compared. Films with 20%wt copper nanowires showed R_s=11.8 Ω/□ with T=81.4% at 550nm. But altogether no enhancement or advantage can be stated for combining copper and silver nanowires in one combined random network.

4.3 DEVICE INTEGRATION

After establishing well performing AgNW electrodes, the consequent step is integration in full devices.

4.3.1 Materials

Common and well tested materials are used in the device to minimize variables. Regioregular P3HT (4002-EE) and PCBM ($PC_{60}BM$) were purchased from Rieke Metals Inc. and Nano-C Inc., respectively, and used as received. Poly(3,4-ethylenedioxythiophene):poly(styrene sulfonate) (PEDOT:PSS) (Baytron P) and Chlorobenzene (Aldrich, 99.8%) are also used as received.

A solution of P3HT:PCBM with a weight ratio of 1:0.8 and a concentration of 35 mg/mL was dissolved in chlorobenzene under agitation.

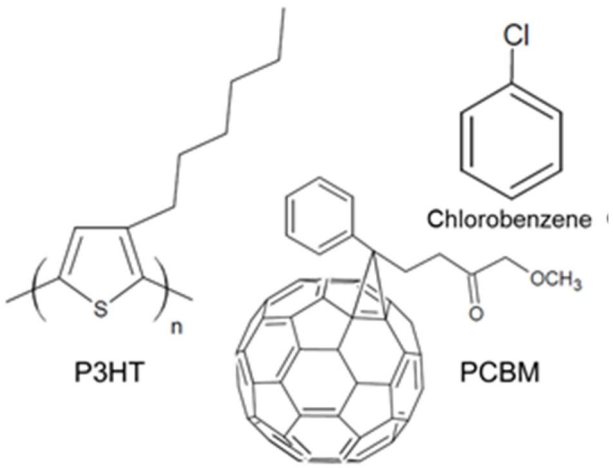

Figure 27 Chemical structures of P3HT, PCBM and chlorobenzene

4.3.2 Device Fabrication

ITO-coated glass and bare glass substrates are cleaned by ultrasonication in acetone, isopropyl alcohol and de-ionized water, and subsequently dried in an oven

overnight. After 10 minutes of ultraviolet-ozone (UVO) treatment, PEDOT:PSS is spin-coated with a thickness of ~70 nm on top of the AgNW layer or ITO and dried for 30 minutes at 120 °C in vacuum. SiO_2 patterns with either 200 nm or 300 nm thickness are thermally evaporated on top of PEDOT:PSS for both AgNW and ITO samples. Samples without SiO_2 are fabricated as well.

In an Argon filled glove box P3HT:PCBM solution is spin-coated at 2000 rpm for 60 s on top of the PEDOT:PSS/SiO_2 layer, and kept in a glove box for one hour. Afterwards 0.5 nm of LiF and 100 nm of Al layers are thermally evaporated under a 10^{-6} Torr vacuum with a deposition rate of 0.05-0.1 Å/s, and 2-5 Å/s, respectively. After fabrication devices are thermally annealed at 150 °C for 15 minutes in an Argon atmosphere. The device structure is illustrated in Figure 28 Illustration of device structure for OSC.

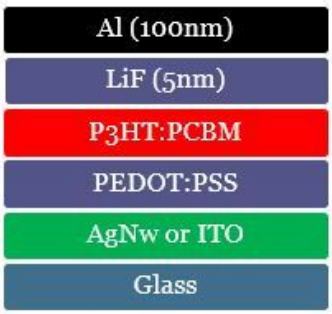

Figure 28 Illustration of device structure for OSC

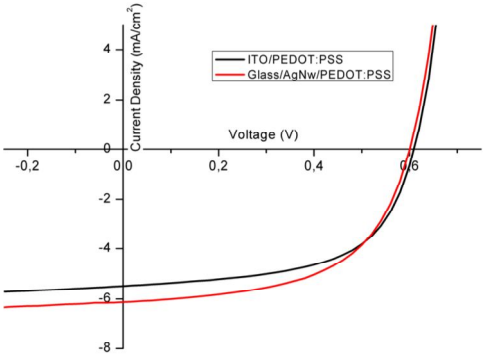

Figure 29 J-V Charactersitic for unpatterned devices based on AgNW (red) and ITO (black) electrodes

4.3.3 Measurement Results

Measurement results for unpatterned photovoltaic cells fabricated with device configuration AgNW(or ITO)/PEDOT:PSS/P3HT:PCBM/LiF/Al are summarized in (Table 3 Device characteristics of unpatterned devices with AgNW and ITO

electrodes).Devices with AgNW electrodes show a slightly higher current density which lead to an average performance increase of 2% compared to devices prepared with ITO bottom electrodes. This performance improvement is attributed to the good electrical properties of the AgNW network as well as light scattering effects of the nanostructures. Light that is reflected on the nanowires into the active layer under a 1-90° angle, travels a longer distance through the active

Experiment: Avg (best)	V_{SC} (V)	I_{SC} (mA)	J_{SC} (mA/cm^2)	FF (%)	η (%)	η Rel. to ITO (Ref.)
ITO/PEDOT:PSS	0.61 (0,61)	0,171 (0,175)	5,45 (5,58)	56,37 (58,53)	1,87 (1,99)	1,00 (1,00)
Glass/AgNw/PEDOT:PSS	0,60 (0,60)	0,178 (0,191)	5,68 (6,08)	55,82 (56,87)	1,90 (2,06)	1,02 (1,04)

Table 3 Device characteristics of unpatterned devices with AgNW and ITO electrodes

material and therefore has a higher chance to be absorbed.

Samples with SiO_2 patterns show a short-circuit behavior and cannot be characterized in terms of performance. Possible causes were suspected in:

1) Overlap of the electrodes on the side area of the samples
2) Contact at the edge of the samples
3) Insufficient thickness of dielectric SiO_2 layer
4) SiO_2 evaporation process damages underlying layer

To avoid the above mentioned possibilities, isolating tape was used on the side of the sample to guarantee separation of the electrodes. The thickness of the SiO_2 layer was increased from 200 nm to 300 nm as well. A change in layer order from

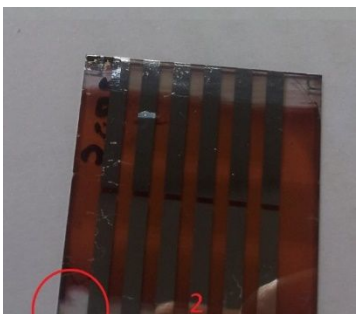

Figure 30 Device areas which possibly cause device malfunction

AgNW/PEDOT:PSS/SiO_2/P3HT:PCBM/LiF/Al to AgNW/SiO_2/ PEDOT:PSS/P3HT:PCBM/LiF/Al did also not solve the defect.

Many more attempts were made to localize the cause for the malfunction without success. Finally SiO_2 patterning method for this purpose was terminated.

5 CONCLUSION

In this thesis, the possible replacement of ITO with silver nanowires in electrodes for organic electronic devices was studied. Therefore electrical and mechanical properties of silver nanowires were analyzed by employing various characterization techniques. Controllable variables were optimized to meet performance requirements for application in devices.

As a result we fabricated silver nanowire networks on glass and flexible plastic substrate which show sheet resistance of 15Ω/□ and transmission of >90% at 550 nm wavelength. Direct comparison of organic solar cells fabricated with silver nanowires to ITO electrodes resulted in a 2% higher performance in silver nanowire based devices. This study demonstrates that the Ag NW electrode meets the most important criteria of conductivity, transparency, flexibility, and solution-processability necessary to replace ITO in organic photovoltaics. Such we anticipate that the application of metal nanowire mesh transparent electrodes to a wide variety of devices, including organic solar cells, will lead to lower cost fabrication and improved performance.

6 REFERENCES

1. Production, R.; Refi, P.; Trade, P. BP Statistical Review of World Energy About this review Contents. **2013**.

2. Harvie, C.; Harvie, C. Export Led Industrialisation and Growth – Korea ' s Economic Miracle 1962-89 University of Wollongong Economic Miracle 1962-89 and. **2003**.

3. Energy Policies of IEA Countries *The Republic of Korea 2012*; 2012.

4. Korean Herald Korea issues contingency plans for fine dust.

5. Wikipedia Green energy http://en.wikipedia.org/wiki/Green_energy.

6. Energy Policies of IEA Countries *The Republic of Korea 2012*; 2012.

7. *Green Energy and Technology*; Amouroux, J., Ed.; Bentham Science Publishers, 2006.

8. Schwoerer, M.; Wolf, H. Organic molecular solids. **2007**.

9. Terao, J.; Wadahama, A.; Matono, A.; Tada, T.; Watanabe, S.; Seki, S.; Fujihara, T.; Tsuji, Y. Design principle for increasing charge mobility of π-conjugated polymers using regularly localized molecular orbitals. *Nat. Commun.* **2013**, *4*, 1691.

10. Petty, M. *Molecular electronics: from principles to practice*; 2007.

11. Song, J. Morphological and Electrical Studies on Additive Solvent-Induced P3HT : PCBM Bulk Heterojunction Organic Solar Cells Abstract Morphological and Electrical Studies on Additive Solvent-Induced P3HT : PCBM Bulk Heterojunction Organic Solar Cells. **2013**.

12. Organic Photovoltaics - Wiley Online Library http://onlinelibrary.wiley.com/book/10.1002/9783527623198 (accessed Apr 29, 2014).

13. Mihailetchi, V. D.; Blom, P. W. M.; Hummelen, J. C.; Rispens, M. T. Cathode dependence of the open-circuit voltage of polymer:fullerene bulk heterojunction solar cells. *J. Appl. Phys.* **2003**, *94*, 6849.

14. Mihailetchi, V. D.; Koster, L. J. A.; Blom, P. W. M. Effect of metal electrodes on the performance of polymer:fullerene bulk heterojunction solar cells. *Appl. Phys. Lett.* **2004**, *85*, 970.

15. Krebs, F. C.; Jørgensen, M.; Norrman, K.; Hagemann, O.; Alstrup, J.; Nielsen, T. D.; Fyenbo, J.; Larsen, K.; Kristensen, J. A complete process for production of flexible large area polymer solar cells entirely using screen printing—First public demonstration. *Sol. Energy Mater. Sol. Cells* **2009**, *93*, 422–441.

16. Kumar, A.; Zhou, C. The race to replace tin-doped indium oxide: which material will win? *ACS Nano* **2010**, *4*, 11–4.

17. Kim, Y. H.; Sachse, C.; Machala, M. L.; May, C.; Müller-Meskamp, L.; Leo, K. Highly Conductive PEDOT:PSS Electrode with Optimized Solvent and Thermal Post-Treatment for ITO-Free Organic Solar Cells. *Adv. Funct. Mater.* **2011**, *21*, 1076–1081.

18. Yu, G.; Cao, A.; Lieber, C. M. Large-area blown bubble films of aligned nanowires and carbon nanotubes. *Nat. Nanotechnol.* **2007**, *2*, 372–7.

19. Lee, M.-S.; Lee, K.; Kim, S.-Y.; Lee, H.; Park, J.; Choi, K.-H.; Kim, H.-K.; Kim, D.-G.; Lee, D.-Y.; Nam, S.; Park, J.-U. High-performance, transparent, and stretchable electrodes using graphene-metal nanowire hybrid structures. *Nano Lett.* **2013**, *13*, 2814–21.

20. Tokuno, T.; Nogi, M.; Jiu, J.; Suganuma, K. Hybrid transparent electrodes of silver nanowires and carbon nanotubes: a low-temperature solution process. *Nanoscale Res. Lett.* **2012**, *7*, 281.

21. Lee, J.-Y.; Connor, S. T.; Cui, Y.; Peumans, P. Semitransparent organic photovoltaic cells with laminated top electrode. *Nano Lett.* **2010**, *10*, 1276–9.

22. Wikipedia Conductivity of metals http://en.wikipedia.org/wiki/Electrical_resistivity_and_conductivity.

23. O'Connor, B.; Haughn, C.; An, K.-H.; Pipe, K. P.; Shtein, M. Transparent and conductive electrodes based on unpatterned, thin metal films. *Appl. Phys. Lett.* **2008**, *93*, 223304.

24. Camacho, J. M.; Oliva, A. I. Surface and grain boundary contributions in the electrical resistivity of metallic nanofilms. *Thin Solid Films* **2006**, *515*, 1881–1885.

25. Kang, M.-G.; Guo, L. J. Nanoimprinted Semitransparent Metal Electrodes and Their Application in Organic Light-Emitting Diodes. *Adv. Mater.* **2007**, *19*, 1391–1396.

26. Krebs, F. C. Roll-to-roll fabrication of monolithic large-area polymer solar cells free from indium-tin-oxide. *Sol. Energy Mater. Sol. Cells* **2009**, *93*, 1636–1641.

27. Lee, J.-Y.; Connor, S. T.; Cui, Y.; Peumans, P. Solution-processed metal nanowire mesh transparent electrodes. *Nano Lett.* **2008**, *8*, 689–92.

28. De, S.; Higgins, T.; Lyons, P. Silver nanowire networks as flexible, transparent, conducting films: extremely high DC to optical conductivity ratios. *ACS …* **2009**, *3*, 1767–1774.

29. Sun, Y.; Yin, Y.; Mayers, B. T.; Herricks, T.; Xia, Y. Uniform Silver Nanowires Synthesis by Reducing AgNO 3 with Ethylene Glycol in the Presence of Seeds and Poly(Vinyl Pyrrolidone). *Chem. Mater.* **2002**, *14*, 4736–4745.

30. Tang, X.; Tsuji, M.; Jiang, P.; Nishio, M.; Jang, S.-M.; Yoon, S.-H. Rapid and high-yield synthesis of silver nanowires using air-assisted polyol method with chloride ions. *Colloids Surfaces A Physicochem. Eng. Asp.* **2009**, *338*, 33–39.

31. Chen, D.; Qiao, X.; Chen, J. Morphology-controlled synthesis of silver nanostructures via a solvothermal method. *J. Mater. Sci. Mater. Electron.* **2011**, *22*, 1335–1339.

32. Tsuji, M.; Hashimoto, M.; Nishizawa, Y.; Kubokawa, M.; Tsuji, T. Microwave-assisted synthesis of metallic nanostructures in solution. *Chemistry* **2005**, *11*, 440–52.

33. Sun, Y.; Mayers, B.; Herricks, T.; Xia, Y. Polyol Synthesis of Uniform Silver Nanowires: A Plausible Growth Mechanism and the Supporting Evidence. *Nano Lett.* **2003**, *3*, 955–960.

34. Gao, Y.; Jiang, P.; Liu, D. F.; Yuan, H. J.; Yan, X. Q.; Zhou, Z. P.; Wang, J. X.; Song, L.; Liu, L. F.; Zhou, W. Y.; Wang, G.; Wang, C. Y.; Xie, S. S.; Zhang, J. M.; Shen, D. Y. Evidence for the Monolayer Assembly of Poly(vinylpyrrolidone) on the Surfaces of Silver Nanowires. *J. Phys. Chem. B* **2004**, *108*, 12877–12881.

35. Lee, J. H.; Lee, P.; Lee, D.; Lee, S. S.; Ko, S. H. Large-Scale Synthesis and Characterization of Very Long Silver Nanowires via Successive Multistep Growth. *Cryst. Growth Des.* **2012**, *12*, 5598–5605.

36. Pike, G.; Seager, C. Percolation and conductivity: A computer study. I. *Phys. Rev. B* **1974**, *10*, 1421–1434.

37. Mutiso, R.; Sherrott, M.; Rathmell, A. Integrating Simulations and Experiments To Predict Sheet Resistance and Optical Transmittance in Nanowire Films for Transparent Conductors. *ACS …* **2013**, 7654–7663.

38. Mutiso, R. M.; Sherrott, M. C.; Rathmell, A. R.; Wiley, B. J.; Winey, K. I. Integrating simulations and experiments to predict sheet resistance and optical transmittance in nanowire films for transparent conductors. *ACS Nano* **2013**, *7*, 7654–63.

39. Madaria, A. R.; Kumar, A.; Ishikawa, F. N.; Zhou, C. Uniform, highly conductive, and patterned transparent films of a percolating silver nanowire network on rigid and flexible substrates using a dry transfer technique. *Nano Res.* **2010**, *3*, 564–573.

40. Bergin, S. M.; Chen, Y.-H.; Rathmell, A. R.; Charbonneau, P.; Li, Z.-Y.; Wiley, B. J. The effect of nanowire length and diameter on the properties of transparent, conducting nanowire films. *Nanoscale* **2012**, *4*, 1996–2004.

41. Yang, L.; Zhang, T.; Zhou, H.; Price, S. C.; Wiley, B. J.; You, W. Solution-processed flexible polymer solar cells with silver nanowire electrodes. *ACS Appl. Mater. Interfaces* **2011**, *3*, 4075–84.

42. Chen, C.; Dou, L.; Zhu, R.; Chung, C.; Song, T.; Zheng, Y. B.; Al, C. E. T. Cells Produced by Solution Processing. **2012**, 7185–7190.

43. Wu, H.; Hu, L.; Rowell, M. W.; Kong, D.; Cha, J. J.; McDonough, J. R.; Zhu, J.; Yang, Y.; McGehee, M. D.; Cui, Y. Electrospun metal nanofiber webs as high-performance transparent electrode. *Nano Lett.* **2010**, *10*, 4242–8.

44. Gaynor, W.; Lee, J.-Y.; Peumans, P. Fully solution-processed inverted polymer solar cells with laminated nanowire electrodes. *ACS Nano* **2010**, *4*, 30–4.

45. Hall, D. B.; Underhill, P.; Torkelson, J. M. Spin coating of thin and ultrathin polymer films. *Polym. Eng. Sci.* **1998**, *38*, 2039–2045.

46. Kim, A.; Won, Y.; Woo, K.; Jeong, S.; Moon, J. All-Solution-Processed Indium-Free Transparent Composite Electrodes based on Ag Nanowire and Metal Oxide for Thin-Film Solar Cells. *Adv. Funct. Mater.* **2014**, n/a–n/a.

47. Gaynor, W.; Burkhard, G. F.; McGehee, M. D.; Peumans, P. Smooth nanowire/polymer composite transparent electrodes. *Adv. Mater.* **2011**, *23*, 2905–10.

48. Zhu, R.; Chung, C.-H.; Cha, K. C.; Yang, W.; Zheng, Y. B.; Zhou, H.; Song, T.-B.; Chen, C.-C.; Weiss, P. S.; Li, G.; Yang, Y. Fused silver nanowires with metal oxide nanoparticles and organic polymers for highly transparent conductors. *ACS Nano* **2011**, *5*, 9877–82.

49. Moon, I. K.; Kim, J. Il; Lee, H.; Hur, K.; Kim, W. C.; Lee, H. 2D Graphene Oxide Nanosheets as an Adhesive Over-Coating Layer for Flexible Transparent Conductive Electrodes. *Sci. Rep.* **2013**, *3*, 1112.

50. Li, G.; Shrotriya, V.; Huang, J.; Yao, Y.; Moriarty, T.; Emery, K.; Yang, Y. High-efficiency solution processable polymer photovoltaic cells by self-organization of polymer blends. *Nat. Mater.* **2005**, *4*, 864–868.

51. Garnett, E. C.; Cai, W.; Cha, J. J.; Mahmood, F.; Connor, S. T.; Greyson Christoforo, M.; Cui, Y.; McGehee, M. D.; Brongersma, M. L. Self-limited plasmonic welding of silver nanowire junctions. *Nat. Mater.* **2012**, *11*, 241–9.

52. Choi, K.; Kim, J.; Noh, Y.; Na, S.; Kim, H. Ag nanowire-embedded ITO films as a near-infrared transparent and flexible anode for flexible organic solar cells. *Sol. Energy Mater. Sol. …* **2013**.

53. Chung, C.-H.; Song, T.-B.; Bob, B.; Zhu, R.; Yang, Y. Solution-processed flexible transparent conductors composed of silver nanowire networks embedded in indium tin oxide nanoparticle matrices. *Nano Res.* **2012**, *3*, 676–684.

54. Ahn, Y.; Jeong, Y.; Lee, Y. Improved thermal oxidation stability of solution-processable silver nanowire transparent electrode by reduced graphene oxide. *ACS Appl. Mater. Interfaces* **2012**, *4*, 6410–4.

55. Kim, A.; Won, Y.; Woo, K.; Kim, C.-H.; Moon, J. A Highly Transparent Low Resistance ZnO/Ag Nanowire/ZnO Composite Electrode for Thin Film Solar Cells. *ACS Nano* **2013**.

56. Chen, C.; Dou, L.; Zhu, R.; Chung, C.; Song, T.; Zheng, Y. B.; Al, C. E. T. Cells Produced by Solution Processing. **2012**.

57. TOKUSEN KOGYO TOKUSEN KOGYO http://www.tokusen.co.jp/en/index.php.

58. Xin Yan Technology Xin Yan Technology Limited http://www.xinyan.hk/list/?106_1.html.

59. Mayousse, C.; Celle, C.; Carella, A.; Simonato, J. Synthesis and purification of long copper nanowires. Application to high performance flexible transparent electrodes with and without PEDOT: PSS. *Nano Res.* **2013**.

60. CNVISION CO., L. CNVISION CO.,LTD http://cnvision.co.kr/.

61. Wikipedia Economy of South_Korea http://en.wikipedia.org/wiki/Economy_of_South_Korea.

62. Leo, P. D. K. Organic Semiconductor World http://www.iapp.de/orgworld/?Basics:What_are_organic_semiconductors.

63. Kumar, A.; Zhou, C. The race to replace tin-doped indium oxide: which material will win? *ACS Nano* **2010**, *4*, 11–4.

64. De, S.; King, P. J.; Lyons, P. E.; Khan, U.; Coleman, J. N. Size effects and the problem with percolation in nanostructured transparent conductors. *ACS Nano* **2010**, *4*, 7064–72.

65. Spin Coat Theory http://www.clean.cise.columbia.edu/process/spintheory.pdf.

7 초록 (ABSTRACT IN KOREAN)

투명 전극은 광전자소자에서 필수적인 요소이다. 유기태양전지의 투명 전극으로 주로 사용되는 ITO(Indium Tin Oxide, 인듐주석산화물)는 높은 재료 비용, 높은 공정 온도와 낮은 기계적 내구성으로 상업성의 측면에서 좋지 않다. 그러므로 이러한 ITO를 대체할 투명전극으로써 전도성 고분자, 금속 나노선, 탄소나노튜브 등에 관한 연구가 유기전자소자 분야에서 활발히 진행되고 있다. 이 중에서도 은 나노선을 이용한 전극은 좋은 전도성을 보일 뿐 아니라 높은 기계적 내구성 및 광학적 투과도를 나타낸다. 따라서 낮은 재료 비용 및 낮은 공정 단가와 결합하여 은 나노선 네트워크는 ITO를 대체할만한 가장 유망한 투명 전극 물질이다.

본 논문에서는 은 나노선의 기본적인 합성에서 시작하여 유기태양전지의 소자 적용에 이르기까지의 연구를 다루었다. 은 나노선의 물리적인 네트워크 구조나 공정 방법 등을 연구하였고, 실제 유기태양전지 소자의 투명 전극에 적용하는 데에 있어서 물질적인 특성이나 소자의 특성 평가 연구도 진행하였으며, 또한 앞으로 극복해 나가야 할 도전적인 문제들도 함께 제시하였다. 은 나노선 전극을 패터닝할 수 있는 방법 및 특성을 향상시킬 수 있는 방법들도 소개하고자 한다. 결과적으로, 저비용, 유연함을 가지는 은 나노선 전극을 사용하여 ITO와 비슷한 수준의 특성을 보이는 유기태양전지를 구현하였다. 본 논문을 통해 은 나노선 네트워크에서의 동작원리에 대한 이해 및 향후 유연한 유기태양전지 소자 제작에 도움이 될 것이라 생각한다.

주요어: 유기 태양전지, 투명 전극, 은 나노선

학 번: 2012-23965